ACS Catalysis

Research Article

pubs.acs.org/acscatalysis

Comparative Study of Imidazole and Pyridine Catalyzed Reduction of Carbon Dioxide at Illuminated Iron Pyrite Electrodes

Andrew B. Bocarsly,* Quinn D. Gibson, Amanda J. Morris, Robert P. L'Esperance, Zachary M. Detweiler, Prasad S. Lakkaraju, Elizabeth L. Zeitler, and Travis W. Shaw

Frick Chemical Laboratory, Princeton University, Princeton, New Jersey 08544, United States

Supporting Information

ABSTRACT: The chemistry of the electrocatalytic reduction of CO_2 using nitrogen containing heteroaromatics is further explored by the direct comparison of imidazole and pyridine catalyzed CO_2 reduction at illuminated iron pyrite electrodes. The mechanism of imidazole based catalysis of CO_2 reduction is investigated by analyzing the catalytic activity of a series of imidazole derivatives using cyclic voltammetry. While similar product distributions are obtained for both imidazole and pyridine, the imidazole catalyzed reduction of CO_2 likely proceeds via a very different mechanism involving the C2 carbon of the imidazole ring.

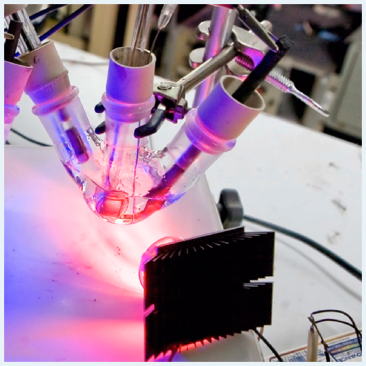

KEYWORDS: *photoelectrochemistry, aromatic amine electrocatalysts, carbon dioxide reduction, iron pyrite photocathodes, imidazolium based electrocatalyst, pyridinium based electrocatalysis, formic acid production*

INTRODUCTION

Recent attention has focused on new methods to ameliorate the amounts of carbon dioxide placed into the atmosphere by fossil fuel combustion because of concerns about anthropogenically induced climate change. The capture and conversion of CO_2 into a value added product, for example, as plastic precursors or liquid fuels, has been proposed.[1] The reduction of CO_2 is energy intensive and, therefore, the overall balance of energy in such conversion is of major concern. One of the major contributions to the overall energy balance is the typically high overpotential associated with the multielectron reduction of CO_2. Thus, efficient catalysis of this reaction is essential.

CO_2 reduction at various metals in aqueous solution has been exhaustively studied by Hori and others.[2] Although a variety of organic products have been reported, all systems investigated exhibited a combination of high overpotential, poor faradaic efficiency, and limited system stability. In aqueous solution, under standard conditions, copper is the only electrode material that has any efficiency for highly reduced carbon products, but here again the potentials required (at least −1.7 V vs SCE), along with the reported low faradaic yields and limited electrode stability, render this system of limited practical interest.[3] CO_2 reduction has also been observed at several metal surfaces in nonaqueous electrolyte (Pb, Hg, Tl, Pt, Ni, Fe, Cr, Mo, Pd, Cd, Ti, Nb) but these reactions also required the application of extremely negative potential (negative of −2.5 V vs SCE).[4]

Our group has reported on the pyridinium-catalyzed reduction of CO_2 at illuminated p-GaP photoelectrodes selectively to methanol at an underpotential.[5] The mechanism of the reactivity was investigated at platinum electrodes.[6] To date, this approach remains the most energy efficient process for reduction of CO_2 to organic products. In the proposed mechanism, the rate-determining formation of a radical carbamate species, via the bimolecular reaction of a one electron reduced pyridinyl radical with CO_2, is followed by steps that involve the interaction of this and other intermediates with the surface of the electrode.[6,7] These surface interactions lead to varying product distributions based on the electrode material employed. For example, methanol is formed with near 100% faradaic efficiency at p-GaP surfaces whereas at Pt electrodes methanol and formic acid are observed with 22% and 11% faradaic efficiency, respectively. Similarly, varying the aromatic amine electrocatalyst can affect the distribution of products, including the formation of carbon−carbon bonded products.[8] This has necessitated the consideration of each catalyst/electrode combination individually. Thus, an understanding of key mechanistic features must be developed.

In contrast to the prior electrode materials studied as cathodes for the aromatic amine/CO_2 system, it is observed that illuminated p-FeS_2 photocathodes selectively undertake the 2-electron reduction of CO_2 to form formic acid or CO. Although restrictive with regard to the pragmatic production of highly reduced organics, limiting the net charge transfer process

Received: April 25, 2012
Revised: June 27, 2012
Published: July 3, 2012

to 2-electrons provides a convenient simplification of the charge transfer mechanism, allowing access to the kinetic details of this process. In prior work, using platinum electrodes to form methanol from CO_2 we identified that the initial 2-electron reduction to formic acid was rate limiting.[6] Thus, an understanding of this process is essential to understanding the overall mechanism associated with the aromatic amine catalyzed formation of alcohols.

In this work, the previously investigated reactivity of pyridines with CO_2 is extended to other aromatic amine catalysts in a comparative study between imidazole and pyridine at iron pyrite (FeS_2) photoelectrodes. Different product distributions are obtained for both aromatic amine catalysts; imidazole reduces CO_2 to a mixture of CO and formic acid at a moderate potential, while pyridine selectively generates formic acid. Interestingly, evidence reported here suggests markedly different mechanisms for pyridinium and imidazolium electrocatalytic activity at both iron pyrite and platinum electrodes. While a carbamate species appears to be a likely intermediate for pyridinium catalyzed CO_2 reduction, it is proposed here that imidazolium reduction produces an imidazolium 2-ylidine intermediate. Though N-heterocylic carbenes (NHC) have been studied extensively in the field of organometallic catalysis, this is, to the best of our knowledge, the first evidence of a simple protonated imidazole reacting via a carbene intermediate.

EXPERIMENTAL SECTION

Materials. Potassium chloride (≥99%, EMD), pyridine (≥99.9%, Aldrich), imidazole (≥99%, Aldrich), 1-ethyl 3-methyl imidazolium bromide, 2-methyl imidazole, sulfuric acid (EMD), nitric acid (EMD), argon (99.8%, Airgas), deuterium oxide (>99.9%, Cambridge Isotope Laboratories Inc.), potassium oxalate (99%, Fisher), sodium formate (>99%, Aldrich), 2,2′-bipyridine (>99%, Aldrich), and carbon dioxide (99.8%, Airgas) were used as received. Single crystal iron pyrite samples were purchased from Wards Natural Science. The back of the electrode crystals were coated with indium−gallium eutectic (>99.99%, Aldrich) and mounted on a bare copper wire with silver epoxy (Epoxy Technologies, EpoTek H31). The wire assembly was encased in a glass tube and coated with insulating epoxy (Locite, Hysol 051) to ensure all chemistry occurred at the exposed pyrite crystal face. Deionized water was used to prepare the aqueous electrolyte solutions.

Material Characterization. *X-ray Crystallography.* Analysis was carried out on a Bruker D8 Advanced High Resolution X-ray diffractometer equipped with a copper long fine focus tube at a monochromatic wavelength of 1.54 Å (1 mm slit width). The X-ray diffraction (XRD) pattern was taken using a standard "θ 2θ" configuration.

XPS. X-ray photoelectron spectroscopy (XPS) data was collected using a VG Scientific magnesium salt anode source at a 15 kV accelerating voltage and a hemispherical sector analyzer detector with a pass energy of 20 eV. Background scans were performed from 1000 to 0 eV, with a step size of 1 eV and a dwell time of 100 ms. Detailed Fe2p scans were performed between 740 and 700 eV, with a step size of 0.1 eV and a dwell time of 300 ms. S2p scans were performed between 175 and 155 eV using the same parameters. A total of 64 scans were averaged in the reported spectra.

Electrochemistry. *Cyclic Voltammograms (CVs).* Polarization curves were collected on either a CH Instruments 760D or 1140A potentiostat. A standard three-electrode arrangement was used with a pyrite working electrode, Pt mesh (Aldrich) counter electrode, and saturated calomel reference electrode (Accumet). The assembly was immersed in an aqueous electrolyte composed of 10 mM catalyst (pyridine or imidazole) and 0.5 M KCl solution. Prior to experiment, the pyrite electrodes were etched with nitric acid and rinsed with deionized water. The electrolyte solution was purged for 10−45 min with Ar or CO_2. To preserve the desired gaseous atmosphere during the experiment, a constant flow of gas was maintained in the cell headspace. CVs were collected over a scan rate range of 5 mV/s to 200 mV/s. All potentials are referenced to the SCE. For experiments carried out under illumination, a PTI 75W Xe source was employed with a pyrex cut off filter. This source provided broadband illumination from 350 nm to 1350 nm with an intensity of 890 mW/cm^2 at the electrode surface.

Bulk Electrolysis. Experiments were carried out in either a H-type, gastight, three-compartment (cathode, salt bridge, anode) electrochemical cell utilizing two porous glass frit separators (Ace Glass), or a three-neck round-bottom flask. In both cases the electrolyte solution was purged for 15−45 min with Ar or CO_2 prior to experiment. For gastight experiments, after the solution was purged, the cell was sealed with Teflon caps. Headspace analysis was conducted through a stopcock port on the working electrode compartment. For these experiments, a pyrite working electrode, Pt mesh counter electrode, and SCE reference were employed. For single compartment bulk electrolysis carried out in a three neck round-bottom, a pyrite working electrode, carbon rod counter electrode, and SCE reference electrode were employed. To preserve the proper gaseous atmosphere, CO_2 or Ar was consistently bubbled through the solution for the entire duration of the experiment. A carbon counterelectrode was utilized. All bulk electrolysis experiments were carried out under illumination using the HgXe source described in the prior section.

NMR. Samples were prepared using 540 μL of reaction solution and 60 μL of D_2O. A gradient-assisted excitation sculpting method for water suppression was applied using an in-house modified pulse sequence from the Bruker library. Typical data acquisition parameters on a Bruker Avance-II spectrometer, equipped with a DCH cryoprobe with z-gradient, include the collection of 32,000 data points over 3.17 s acquisition time, with added 1 s recycle delay and typically 256 scans. The selective Gaussian inversion pulse on the water (4.680 ppm) was 1.2 ms in duration. Temperature was controlled at 295 K.

Gas Chromatography. Analysis was carried out on Hewlett-Packard 5890A Series gas chromatograph with a molsieve column (Agilent 19091P-MS4, 30 m length, 0.320 mm inner diameter, 12 μm film). A gastight syringe (Pressure-Lok) was used to remove 0.7 mL of headspace gas from the bulk electrolysis cell. From the syringed sample, 0.5 mL was injected onto the column that was held isotemp at 30 °C for 7 min. The retention time for carbon monoxide was determined to be ∼2.97 min by injection of known concentration carbon monoxide/hydrogen mixed gases

Ion Chromatography. Analysis was carried out on a Dionex ICS-5000. Water for eluent preparation is from a Milli-Q Direct 8 system that is subsequently vacuum distilled to remove trace CO_2/carbonate. An IonPac AS19 analytical column (4 × 250 mm) with a guard column (4 × 50 mm) was utilized with a column flow of 1 mL/min at a system pressure is ∼2000 psi. The column was equilibrated at a starting eluent concentration

dx.doi.org/10.1021/cs300267y | ACS Catal. 2012, 2, 1684−1692

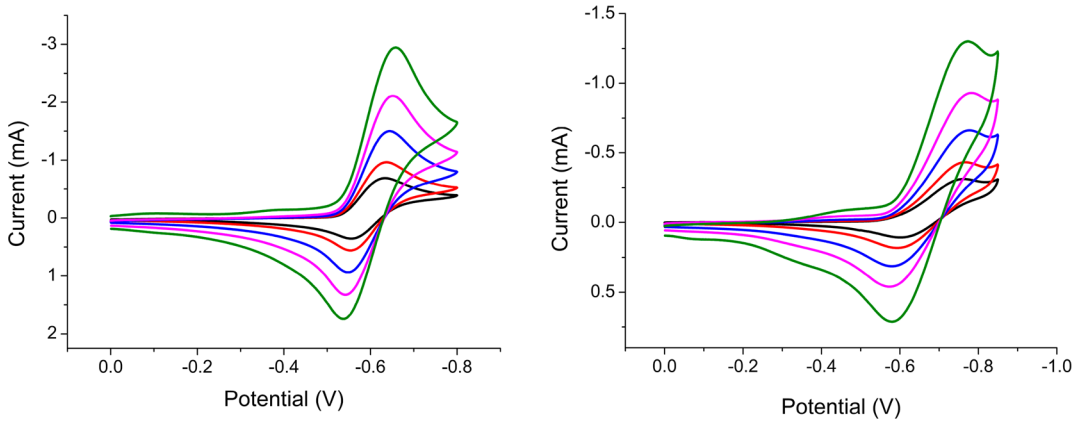

Figure 1. (Left) CVs of 10 mM pyridine in an aqueous solution of 0.5 M KCl at pH 5.3 under an Ar atmosphere at a Pt electrode. (Right) CVs of 10 mM imidazole in an aqueous solution of 0.5 M KCl at pH 5.68 under an Ar atmosphere at a Pt electrode. The scan rates shown are 5 (black), 10 (red), 25 (blue), 50 (magenta), and 100 (green) mV/s.

of 5 mM KOH, held at 5 mM KOH for 10 min, and ramped to 70 mM KOH over 30 min using a multistep gradient. The injection volume was 25 μL. The column and compartment were held at 30 °C. The retention times for formate, chloride, and oxalate are 11.01, 15.5, and 23.12 min, respectively. Limit of detection is <0.1 ppm. For quantitative analysis, calibration curves were generated over the range of interest (0.1−25 ppm).

RESULTS AND DISCUSSION

Cyclic voltammetric measurements of protonated pyridine (at pH 5.3) and protonated imidazole (at pH 5.68) under an Ar atmosphere at a Pt working electrode give one quasi-reversible reduction wave centered at −0.60 V vs SCE in the case of pyridinium and centered at −0.68 V vs SCE for imidazolium (Figure 1). The quasi-reversibility of the system has previously been associated with the formation of hydrogen upon the bimolecular reaction of one electron reduced aromatic amines.[9] The imidazolium CVs also exhibit a small shoulder at ∼−0.4 V vs SCE, which is a prewave associated with imidazole adsorption. The observed reduction potentials overlap well with the reported value of the pyrite conduction band edge, E_{CB} (−0.63 V vs SCE at pH 5.3), indicating that efficient interfacial charge transfer to the amine, with little to no potential loss is thermodynamically possible.[10] In addition, since the reduction potentials of the protonated amines at the pH values employed overlap well with the CO_2 redox states, these systems are energetically well matched to effect the amine mediated catalytic reduction of CO_2.

The reduction of pyridinium at an illuminated pyrite electrode under an Ar atmosphere in 0.5 M KCl aqueous electrolyte adjusted to a pH of 5.3 is shown in Figure 2. The pyridinium reduction at the oriented [100] crystal face of pyrite is irreversible and occurs at more negative potential than at Pt. A similar result is observed for the reduction of imidazole/imidazolium at pyrite. This is likely due to a kinetic barrier to aromatic amine reduction at pyrite electrodes. A similar shift in reduction peak potential has been previously observed for pyridinium at metal electrodes and appears to follow the trend in proton reduction reactivity. The reduction potential is reported to shift more negative in the order Pt < Pd < Au < Ti < Fe < Ni < Cd < Pb < Hg.[9] In this data, there is a hint that the nature of the interaction between the surface and the aromatic amine is important for reduction.

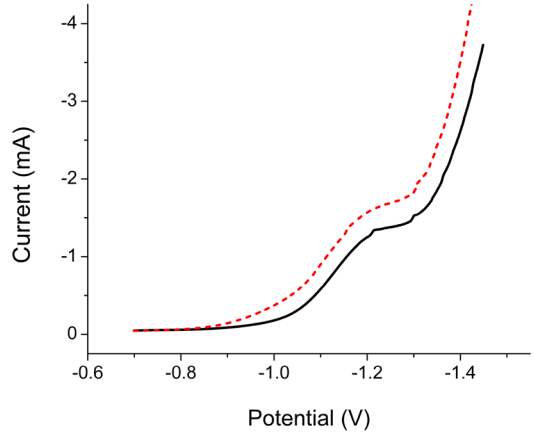

Figure 2. Linear sweep voltammograms (10 mV/s) of 10 mM pyridine in a 0.5 M KCl aqueous solution adjusted to pH = 5.3 under a CO_2 at a dark (black) and illuminated (red dashed) pyrite electrode. The shift in onset potential upon illumination is 77 mV.

The metal-like properties of natural iron pyrite, and thus, its ability to exhibit dark electrode properties have been previously noted.[11] As shown in Figure 2, dark cathodic activity is also observed with the aromatic amine system. Illumination of the electrode (Figure 2) does affect the current−voltage response of the pyrite electrode. As expected for a p-type material, an enhancement in the cathodic current and a positive shift in the current onset potential is observed. The shift in the onset potential was 77 mV as measured at a current of 0.25 mA. This small shift is likely due to the high density of defect states in the natural pyrite samples used in combination with the small band gap of iron pyrite (0.9 eV). These features allow for thermal population of the conduction band at room temperature. The metal like behavior of the p-FeS_2 electrodes utilized justifies the use of standard Nicholson and Shain cyclic voltammetric diagnostics to analyze the mechanism of charge transfer at both dark and illuminated pyrite electrodes. This assertion is further supported by bulk electrolyses at p-FeS_2 electrodes, which were conducted in the dark and in the light at −1.1 V vs SCE. The products observed are identical under both conditions, and the only observable difference is that the rate of reduction was larger for illuminated electrodes. All bulk electrolyses results reported herein are under illuminated conditions.

dx.doi.org/10.1021/cs300267y | ACS Catal. 2012, 2, 1684−1692

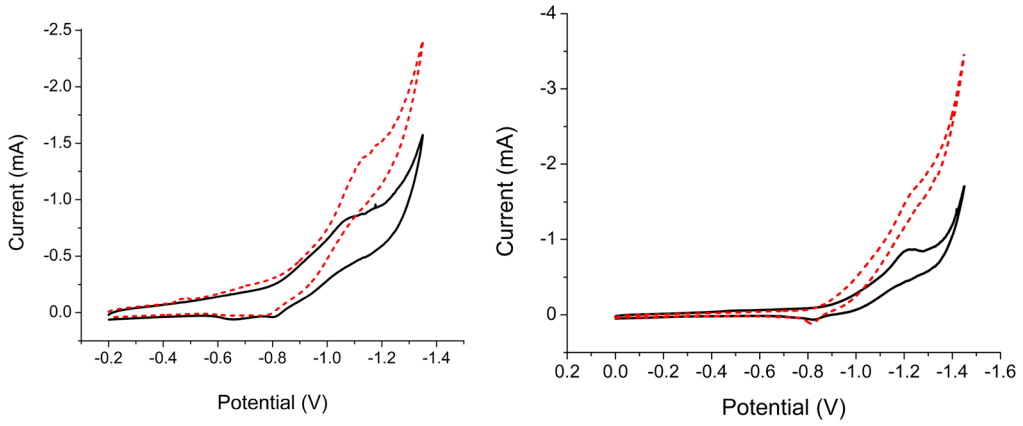

Figure 3. (Left) CVs of 10 mM pyridine in an aqueous solution of 0.5 M KCl at pH 5.3 under an Ar atmosphere (black) and a CO_2 atmosphere (red dashed) at an illuminated pyrite electrode. (Right) CVs of 10 mM imidazole in an aqueous solution of 0.5 M KCl at pH 5.3 under an Ar atmosphere (black) and a CO_2 atmosphere (red dashed) at an illuminated pyrite electrode. The scans were collected at 10 mV/s. The small anodic peak observed at −800 mV in all reported voltammetric sweeps has been attributed to the corrosion of pyrite.[15]

Figure 3 presents CVs of pyridine and imidazole (10 mM) at illuminated pyrite electrodes under a CO_2 atmosphere in 0.5 M KCl containing aqueous electrolyte. The pH of the CO_2 purged solutions are 5.3 for pyridine solutions and 5.68 for imidazole solutions because of the difference in the pK_a of the two aromatic amines (5.14 for pyridine, and 6.95 for imidazole).[12,13] The acid−base interaction between the catalyst and dissolved CO_2 species dictates the observed pH and, in turn, how much catalyst is in the protonated, redox active form. For direct comparison, the CVs collected under an Ar atmosphere were pH-adjusted using HCl or sulfuric acid to the autobuffered pH under CO_2. At constant pH, there is a substantial increase in peak current observed in the presence of CO_2 indicative of catalytic CO_2 reduction.[14] In all pyrite based CVs, a small anodic peak is observed at ∼−800 mV; this is consistent with other literature reports where it has been attributed to the corrosion of pyrite.[15]

For both imidazole and pyridine at a pyrite electrode, the cyclic voltammetric peak current was found to increase linearly with the square root of scan rate under argon and CO_2 (Figure 4 inset). Therefore, the electrochemical process is diffusion limited. Nicholson and Shain diagnostics indicate that the relationship between current and scan rate under a CO_2 atmosphere is due to an underlying electrocatalytic mechanism.[14] A dependence of the peak current on the concentration of amine catalyst employed was carried out. Figure 5 shows the

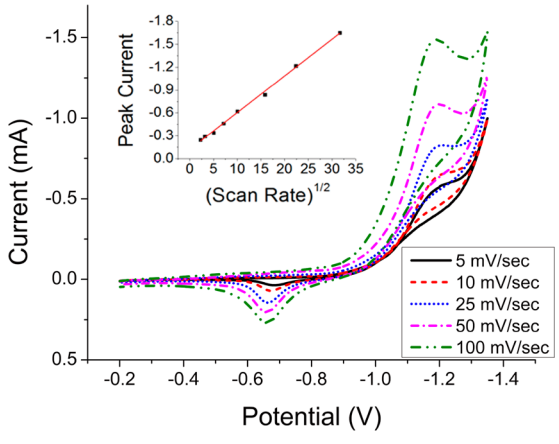

Figure 4. Scan rate dependence of the reduction of pyridine at an illuminated pyrite electrode under a CO_2 atmosphere. (Inset) The linear dependence of cathodic peak current with the square root of the scan rate from 5 to 1000 mV/s indicates a diffusion limited electrochemical reaction.

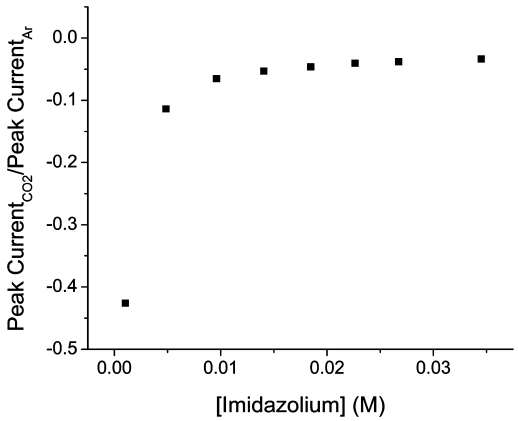

Figure 5. Dependence of the catalytic peak current, reported as the current measured under a CO_2 atmosphere normalized to that measured under an argon atmosphere in a pH-matched solution, on imidazolium concentration. The concentration of imidazolium was corrected for the solution pH.

normalized peak current measured under CO_2 to that measured under argon as a function of imidazolium concentration. The peak current increases until an imidazole concentration of 10 mM at which point the current plateaus. This is consistent with the dependence measured at platinum electrodes for pyridine. It has been proposed that the plateau in current is indicative of a saturation of active surface-sites.[7]

The product distribution from bulk electrolysis at −1.1 V vs SCE was found to be strongly dependent on the aromatic amine catalyst employed. Formic acid was detected after electrolysis in the presence of either pyridine or imidazole (10 mM) by ^{1}H NMR and ion chromatography. Additionally, for imidazole containing electrolytes, carbon monoxide was detected via GC. The faradaic efficiencies for the various products are reported in Table 1. It is important to note that these products only account for <10% of the charge that is passed. Upon application of bias, bubbles are observed at the

dx.doi.org/10.1021/cs300267y | ACS Catal. 2012, 2, 1684−1692

Table 1. Faradaic Efficiencies Calculated for the Various CO_2 Reduction Products Observed at a Pyrite Electrode in the Presence and Absence of Various Amine Catalysts

	faradaic efficiency, %	
	formic acid	carbon monoxide
pyridine, CO_2	2.7 ± 0.2	
imidazole, CO_2	4.9 ± 2.4	2.4 ± 0.1
CO_2	0.2 ± 0.1	trace

electrode surface. Because the observation cannot be accounted for by carbon monoxide formation, the dominant process is assumed to be the reduction of protons to hydrogen in the mildly acidic environment employed.

Pyrite has been previously reported to reduce carbon dioxide upon application of a negative bias.[15,16] Formate production was observed, but only at highly elevated pressures (50 atm) where the maximum faradaic efficiency was reported to be only 0.12% at −1.0 V vs SCE.[15] To confirm that the products observed in the present study are, in fact, due to the action of aromatic amine catalysts, control experiments in the absence of pyridine and imidazole were performed. The CVs of pyrite under Ar and CO_2 atmospheres at a pH of 5.68 are shown in Figure 6. The catalytic current onset occurs at approximately −800 mV vs SCE. This result is consistent with prior results using a rotating disk pyrite electrode.[15]

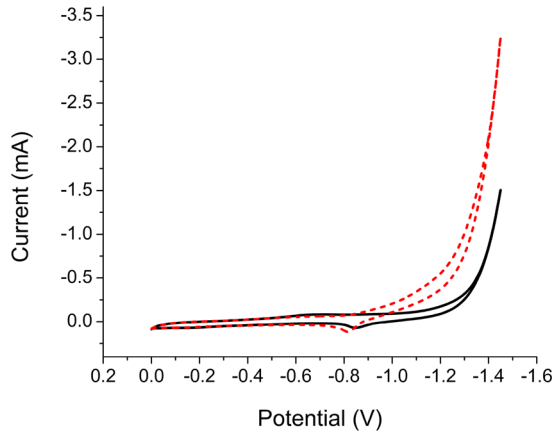

Figure 6. CVs at an illuminated pyrite electrode in an aqueous solution of 0.5 M KCl at pH 5.68 under an Ar atmosphere (black) and a CO_2 atmosphere (red dashed). A 10 mV/s scan rate was employed.

Bulk electrolysis at −1.1 V vs SCE under a CO_2 atmosphere in the absence of a catalyst produced trace carbon monoxide and formic acid as reported in Table 1. The concentration of these products is greatly enhanced during electrolysis in the presence of an amine catalyst. Additionally, for some of the test runs no products were observed when no catalyst was present. That is, in the absence of a catalyst, reduction of CO_2 to CO or formate is minimal and sporadic. Control experiments without CO_2 showed that imidazole can be oxidized to form trace quantities of formate and oxalate through the course of these reactions. Since no oxalate formation was observed to form via the reduction of CO_2, this species was used to monitor crossover from the anode compartment to the pyrite containing cathodic half cell. Control ^{1}H NMR experiments of the catholyte compartment before and after electrolysis demonstrates that the amine catalysts (either pyridine or imidazole) are stable over the duration of the experiment with no breakdown products observed at the level of 1 μM sensitivity.

Given the relative similarity in products observed with both imidazolium and pyridinium catalysts, it was initially hypothesized that catalytic reaction mechanism in both cases utilized similar key intermediates. To evaluate this concept, a variety of imidazole derivatives were tested for catalytic activity. Since electronic arguments suggested that a carbamate radical intermediate, which has been implicated in pyridinium catalysis (eq 1), might be stabilized, in the case of an imidazolium

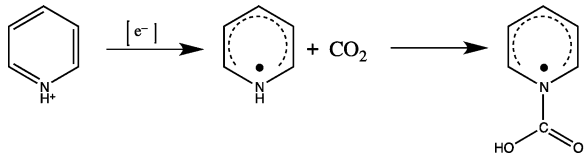

(1)

catalyst by the addition of a methyl group at the C2 position (i.e., the carbon flanked by the two ring nitrogens) this compound was extensively investigated.

CVs of 2-methyl imidazole (10 mM, pK_a = 7.75) at illuminated pyrite electrodes under a CO_2 atmosphere in 0.5 M KCl containing aqueous electrolyte are shown in Figure 7. These voltammograms were performed at pH = 5.6 where ∼95% of the amine is protonated.

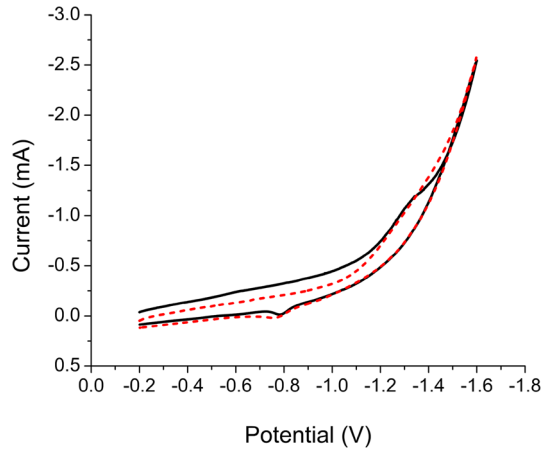

Figure 7. CVs of 10 mM 2-methylimidazole in an aqueous solution of 0.5 M KCl at pH 5.7 under an Ar atmosphere (black) and a CO_2 atmosphere (red dashed) at an illuminated pyrite electrode, performed at 10 mV/s.

While there is a reduction peak at −1.3 V vs SCE indicating the formation of the imidazolium radical, there is no substantial increase in current under CO_2 compared to Ar, indicating that 2-methyl imidazole does not catalyze the reduction of CO_2. The lack of catalytic activity for 2-methyl imidazolium suggests that the interaction between CO_2 and imidazole is at the C2 ring position and not at the ring nitrogens. Thus, a carbamate intermediate is unlikely in the imidazolium system in contrast to the proposed mechanism for pyridine reduction of CO_2.

To further test this latter idea, CVs were performed on 1-ethyl-3-methyl imidazolium bromide, which dissolves in aqueous solution to produce the positively charged 1-ethyl-3-methyl imidazolium ion, wherein both nitrogen atoms in the imidazolium ring are alkylated, and the C2 site is undisturbed. These voltammograms were performed at pH = 3.9, which is the natural pH of the CO_2 saturated system. As shown in

dx.doi.org/10.1021/cs300267y | ACS Catal. 2012, 2, 1684−1692

Figure 8, under argon a poorly resolved reduction peak is observed at −1.3 V vs SCE, which we associate with the

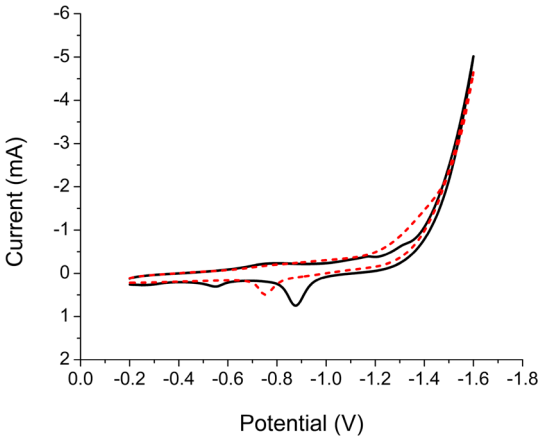

Figure 8. CVs of 10 mM 1-ethyl-3-methyl imidazolium bromide in an aqueous solution of 0.5 M KCl at pH 3.95 under an Ar atmosphere (black) and a CO_2 atmosphere (red dashed) at an illuminated pyrite electrode, performed at 50 mV/s.

reduction of the dialkyl imidazolium. Additionally, there is a modest but distinct increase in the peak current at −1.3 V vs SCE under CO_2 compared to Ar strongly suggesting that the dialkyl imidazolium is catalytic for the reduction of CO_2. This further supports the concept of the C2 carbon as the interaction site. A likely intermediate in the imidazolium case is the ylide, since protonated imidazole greatly resembles the precursors to N-heterocylic carbenes.[17] Thus, the observed electrocatalytic activity of pyridiniums and imidazoliums for the activation of CO_2 following the first electron transfer occurs via distinct and relatively unrelated mechanisms, the former occurring via a carbamate intermediate, and the latter involving what appears to be nucleophilic attack on the CO_2 carbon via an NHC or "ylide-like" electronic structure formed at the C2 ring position. While we believe this conclusion to be chemically reasonable, given the data available and the known reactivity of imidazole, the actual existence of a C2 carbene has not been established at this time. However, the electrochemical generation of an NHC from dialkyl-imidazoliums is supported by Clyburne's observation that electroreduction of 1,3-bis-(2,4,6-trimethylpheny)imidazolium in an ionic electrolyte produces the related 2-ylidene as a persistent species.[18] Using this scenario, the formation of formic acid is then proposed to proceed through a two-electron reduction and proton transfer to the carbon bonded species, eq 2a:

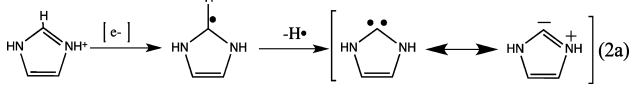

It is unlikely that this proposed mechanism occurs as a pure solution process in an aqueous electrolyte. Thus, a key role for the electrode surface is anticipated, both in stabilizing the zwitterionic resonance structure in eqs 2a−2b, and in the

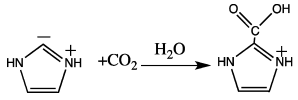

lumped processes associated with 2c. This latter equation is provided for stoichiometric completeness, and not as a

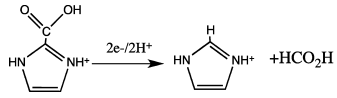

mechanistic proposal. However, we note that the reactivity proposed in this equation is supported by Zhang and Ying's findings that NHCs can bind CO_2 and convert this moiety to alcohols.[19] Recently, Yu and Zhang[20] have reported that certain copper−NHC complexes catalyze the transfer of CO_2 to alkynes to form carboxylic acids via a mechanism that is similar to the surface supported mechanism suggested here, and Tommasi et al. have reported that similar chemistry occurs directly from nonbound NHC compounds.[21] As discussed later in this paper, under operational conditions, the iron pyrite electrode does slowly decompose to produce dissolved ferrous ions. This species might also be involved in the stabilization of the proposed N-heterocyclic carbene intermediate. Intentional addition of Fe(II) to the electrolyte does not alter the product distribution, suggesting, but not proving, that a Fe(II)-imidazole complex is not critical to the reaction pathway. Likewise photolysis of a control solution containing a CO_2 purged imidazolium electrolyte containing 10 mM Fe(II) failed to produce formate ruling out a direct photochemical reduction of CO_2 by imidazole, Fe(II) or an iron imidazole complex.

An equally viable alternative to the EC-based mechanism proposed above is a CE-type mechanism in which the NHC−CO_2 adduct is first formed via a purely solution chemical process and this species is then electrochemically reduced to generate formate as illustrated in eq 3a.

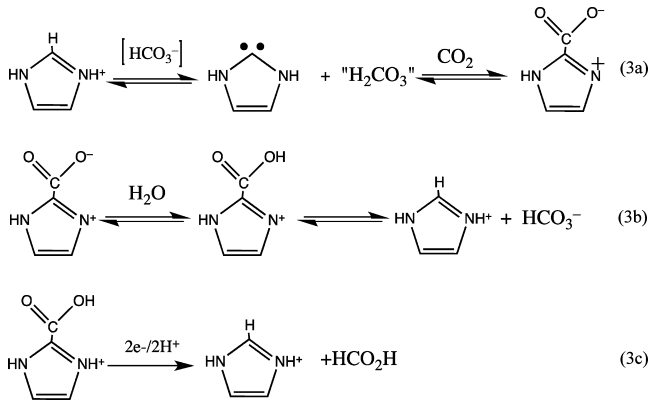

Reaction 3a has recently been reported by Vignolle, Taton, and coworkers using a 1,3-dialkyl imidazolium and methanol solution.[22] The reaction is facile, occurring at room temperature. In this reaction a chemical reduction step is not required to activate the imidazolium. Rather, a series of equilibria produce the 2-ylidene under exceptionally mild conditions, and the carbonylation of this species generates the electroactive intermediate leading to formate.

Although formic acid has been previously proposed as an intermediate in the formation of methanol from CO_2 by pyridine at Pt electrodes, methanol is not observed as a product when p-FeS_2 is used as a cathode. To further investigate this phenomenon, cyclic voltammetry of pyridine and imidazole was carried out in the presence of sodium formate at the reaction pH, 5.3 and 5.68, respectively. Neither catalyst showed an

dx.doi.org/10.1021/cs300267y | ACS Catal. 2012, 2, 1684−1692

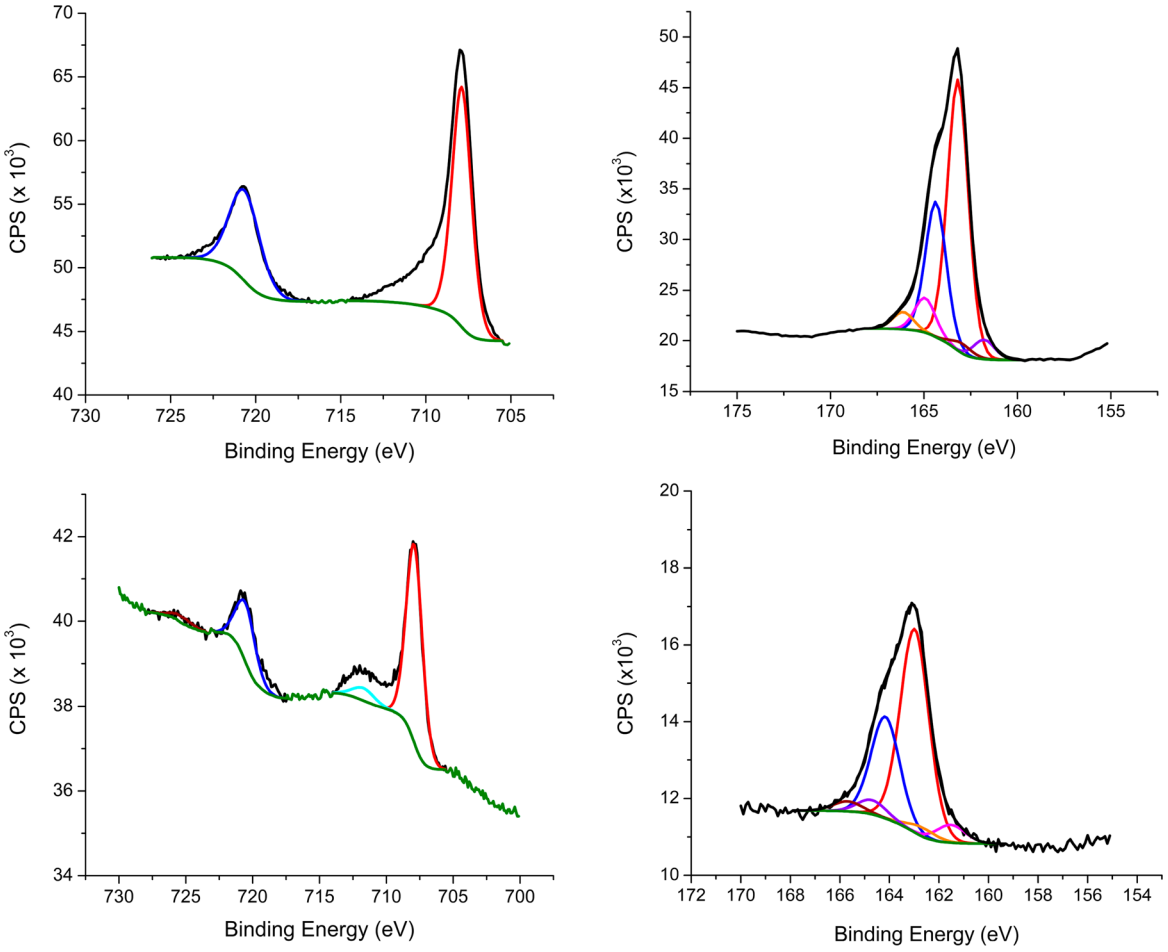

Figure 9. (Top Left) XPS spectrum of the iron 2p region for an etched electrode. (Top Right) XPS spectrum of the sulfur 2p region for an etched electrode. (Bottom Left) XPS spectrum of the iron 2p region for an electrode utilized in the CO_2 reduction reaction in the presence of imidazole at −1.1 V vs SCE. (Bottom Right) XPS spectrum of the sulfur 2p region for an electrode utilized in the CO_2 reduction reaction in the presence of imidazole at −1.1 V vs SCE. The iron region curves are fit to a good approximation as a combination of the Fe $2p_{3/2}$ (red) and Fe $2p_{1/2}$ (blue) of FeS_2, the Fe $2p_{3/2}$ (cyan), and Fe $2p_{1/2}$ (brown) in FeS. The sulfur region curves are fit to a good approximation as a combination of the disulfide S $2p_{3/2}$ (red) and S $2p_{1/2}$ (blue), the polysulfide S $2p_{3/2}$ (purple) and S $2p_{1/2}$ (brown), and the monosulfide S $2p_{3/2}$ (magenta) and S $2p_{1/2}$ (orange).

enhancement of current in the presence of formate. This indicates that the further reduction of formic acid to formaldehyde or methanol is not kinetically possible in the case of iron pyrite with pyridine or imidazole. Once again, this indicates a key role for the electrode surface in the production of multielectron reduced products.

To determine the effect of the surface on the catalytic activity of the aromatic amine, CVs were obtained using 2-methyl imidazole and 1-ethyl-3-methyl imidazolium bromide on platinum at the same pH values employed for the p-FeS_2 electrodes. Both produced ill-defined CVs with a current onset for 1-ethyl-3-methyl imidazolium at −0.8 V vs SCE and an onset of −0.7 V vs SCE for 2-methyl imidazolium. As in the case of a pyrite electrode, only the 1-ethyl-3-methyl imidazolium showed an enhanced current when exposed to CO_2. Thus, the carbamate radical intermediate proposed for pyridinium reduction of CO_2 is not present for imidazole at either platinum or pyrite electrodes. The C2 carbon is likely the active site independent of surface.

We have previously observed in the case of platinum versus p-GaP and p-GaAs electrodes that the same amine catalyst produces different products and different product yields as the electrode material is varied. Here we also see that the products of pyridinium catalyzed reduction of CO_2 differ at pyrite compared to platinum, further strengthening the case that the products observed depend on the electrode surface as much as the amine catalyst employed. Therefore, the surface composition of the pyrite is of great interest. At highly reducing potentials the reduction of pyrite to iron metal and hydrogen sulfide has been reported, eqs 4 and 5.[15]

$$FeS_2 + 2H^+ + 2e^- \rightarrow FeS + H_2S \quad (4)$$

$$FeS + H^+ + 2e^- \rightarrow Fe^0 + HS^- \quad (5)$$

To investigate the surface composition of the pyrite electrodes, XPS of the surface before and after electrolysis was carried out (Figure 9). Pyrite is known for an intensity tailing region, which has been discussed, and rigorously interpreted elsewhere.[23,24] For the purposes of qualitatively assessing the presence of FeS and Fe^0 signals, the tailing region was overlooked. The XPS spectrum of the iron region of an etched pyrite sample shows the presence of peaks that can be attributed to the Fe $2p_{3/2}$ and $2p_{1/2}$ states of FeS_2. The sulfur region of the etched sample spectrum shows the presence of the $2p_{3/2}$ and $2p_{1/2}$ monosulfide, disulfide, and polysulfide states of sulfur in FeS_2 as discussed elsewhere.[24] After electrolysis, the intensity of the signals in the iron and sulfur regions decreased

dx.doi.org/10.1021/cs300267y | ACS Catal. 2012, 2, 1684−1692

significantly because of organic residues on the substrate from electrolysis. Additionally, low intensity peaks that can be attributed to Fe(II) in FeS or iron oxide are observed. There was no evidence of Fe^0 present on the surface. However, since the XPS study necessitates removing the electrode from the electrochemical cell and exposing it to air, the possibility exists that a small amount of a Fe^0 product could have been oxidized prior to the XPS examination. The sulfur region showed an increase in disulfide content in relation to the monosulfide and polysulfide species. This behavior has been reported in previous studies and is attributed to the oxidation of monosulfide to disulfide because of air oxidation. These results are consistent with previous studies.[25,26]

The catholyte was also tested post-electrolysis, and the presence of dissolved iron ions was detected using 10 mM 2,2′-bipyridine as a colorimetric indicator. Although both the XPS results and the presence of Fe^{II} ions in solution indicate the instability of the pyrite photoelectrodes, it is important to note that in the present study the pyrite electrodes were used multiple times without loss in reactivity or product yield. The etch procedure employed between experiments removed any FeS formed upon extended electrolysis.

CONCLUSIONS

While the formation of formic acid and carbon monoxide by the aromatic amines studied was initially thought to proceed through the formation of a carbamate radical, the results obtained for 2-methylimidazole and 1-ethyl-3-methyl imidazolium bromide suggest a much different mechanism for imidazole and its derivatives. Imidazole does not go through a carbamate intermediate, but more likely through an imidazolium 2-ylidine, which forms a carbon−carbon bond with CO_2 to form an imidazolium 2-carboxylate. This type of reactivity has been previously noted in a wide variety of nonaqueous solvents with dialkyl-imidazoliums,[18] and more critical to the current work, by implication in aqueous systems where a 2-ylidine intermediate has been invoked in H-D exchange at the C2 position of imidazolium in D_2O solvent.[27] It is interesting to note that Amyes et al. provide strong thermochemical arguments based on NMR isotope exchange experiments for the aqueous NHC to be in a singlet ground state. Since this species is nucleophilic (being well represented by the resonance structure highlighted in eqs 2a and 2b, its presence is consistent with the observed reactivity of imidazolium toward CO_2. The proposed imidazolium 2-ylidine intermediate might be stabilized by bonding to the metal surface. Such a proposed intermediate is consistent with the literature, where it has been reported that *N*,*N*′-dimethylated imidazole has been shown to bond more strongly to Cu(I) through the carbon when compared to the nitrogen N-methylated imidazole.[20] A similar preference might be exhibited at other surfaces, including the surface iron ions of pyrite. Furthermore, N-heterocyclic carbenes have been shown to have similar π−accepting ability to pyridine when bonded to Fe(II).[28] N-heterocyclic carbenes have also recently been explored as catalysts for carboxylation when in the presence of a Cu(I) metal center.[20]

Although, we put forth an ylide based mechanism as the mostly likely process, other pathways are viable given the available data. For example, the imidazolium ion could react with CO_2 in a concerted fashion, and then be reduced in a CE type mechanism. This would be consistent with the observation that there is not a well-defined reduction peak in the voltammogram of 1-ethyl-3-methyl imidazolium in the absence of carbon dioxide. The fact that the catalytic activity of imidazolium itself is greater than that of 1-ethyl-3-methyl imidazolium suggests that the nitrogens may also participate, either with the binding to CO_2 as an intermediate, or by interactions with the electrode surface or a water molecule. Alternatively, one could also imagine a mechanism in which the imidazole acts as a hydride donor, which directly reduces CO_2 to formic acid. Further detailed mechanistic and kinetic studies need to be undertaken to resolve these ambiguities.

Since 1,3-dialkylimidazolium-2-carboxylates have been previously shown to transfer CO_2 to various alcohols including propargylic alcohol and glycerol,[29] the observation of a similar species in the current study causes us to consider the possibility that these carboxylate intermediates might be used to form carbon−carbon bonded products from CO_2. Carbon−carbon bond formation has been observed previously using a pyridinium catalyst,[8,30] and may be accessible via an imidazolium catalyst based on the mechanistic analysis provided here.

ASSOCIATED CONTENT

Supporting Information

These two files contain original ChemDraw formatted schemes using the ACS ChemDraw format for Schemes 1 and 2 in the manuscript. This material is available free of charge via the Internet at http://pubs.acs.org.

AUTHOR INFORMATION

Corresponding Author

*E-mail: bocarsly@princeton.edu.

Funding

This Article is based upon work supported by the Air Force Office of Scientific Research under AFOSR Award No. FA9550-10-1-0157.

Notes

The authors declare no competing financial interest.

REFERENCES

(1) Aresta, M.; Bocarsly, A. B. *Carbon Dioxide as Chemical Feedstock*; Wiley-VCH Verlag GmbH & Co.: Weinheim, Germany, 2010.
(2) Hori, Y. *Mod. Aspects Electrochem.* **2008**, *42*, 89.
(3) Hori, Y.; Wakebe, H.; Tsukamoto, T.; Koga, O. *Electrochim. Acta* **1994**, *39*, 1833.
(4) Ikeda, S.; Takagi, T.; Ito, K. *Bull. Chem. Soc. Jpn.* **1987**, *60*, 2517.
(5) Barton, E. E.; Rampulla, D. M.; Bocarsly, A. B. *J. Am. Chem. Soc.* **2008**, *130*, 6342.
(6) Barton, C. E.; Lakkaraju, P. S.; Rampulla, D. M.; Morris, A. J.; Abelev, E.; Bocarsly, A. B. *J. Am. Chem. Soc.* **2010**, *132*, 11539.
(7) Morris, A. J.; McGibbon, R. T.; Bocarsly, A. B. *ChemSusChem* **2011**, *4*, 191.
(8) Keets, K.; Morris, A.; Zeitler, E.; Lakkaraju, P.; Bocarsly, A. In *Proceedings of SPIE*; The International Society for Optical Engineering: San Diego, CA, 2010; p 77700.
(9) *Encyclopedia of Electrochemistry of the Elements*; Bard, A. J., Ed.; Marcel Dekker, Inc: New York, 1973; Vol. *15*.
(10) Ennaoui, A.; Tributsch, H. *Sol. Energy Mater.* **1986**, *14*, 461.
(11) Jaegermann, W.; Tributsch, H. *J. Appl. Electrochem.* **1983**, *13*, 743.
(12) Bruice, T. C.; Schmir, G. L. *J. Am. Chem. Soc.* **1958**, *80*, 148.
(13) Brown, H. C. *Determination of Organic Structures by Physical Methods*; Academic Press: New York, 1955.
(14) Nicholson, R. S.; Shain, I. *Anal. Chem.* **1964**, *36*, 706.

(15) Vladimirov, M. G.; Ryzhkov, Y. F.; Alekseev, V. A.; Bogdanovskaya, V. A.; Otroshchenko, V. A.; Kritsky, M. S. *Origins Life Evol. Biospheres* **2004**, *34*, 347.
(16) Tributsch, H.; Fiechter, S.; Jokisch, D.; Rojas-Chapana, J.; Ellmer, K. *Origins Life Evol. Biospheres* **2003**, *33*, 129.
(17) Herrmann, W.; Köcher, C. *Angew. Chem.* **1997**, *36*, 2162.
(18) Gorodetsky, B.; Ramnial, T.; Branda, N.; Clyburne, J. *Chem. Commun.* **2004**, 1972.
(19) Riduan, S. N.; Zhang, Y.; Ying, J. Y. *Angew. Chem.* **2009**, *121*, 3372.
(20) Yu, D.; Zhang, Y. *Proc. Natl. Acad. Sci.* **2010**, *107*, 20184.
(21) Tommasi, I.; Sorrentino, F. *Tetrahedron Lett.* **2009**, *50*, 104.
(22) Fèvre, M.; Pinaud, J.; Leteneur, A.; Gnanou, Y.; Vignolle, J.; Taton, D.; Miqueu, K.; Sotiropoulos, J. M. *J. Am. Chem. Soc.* **2012**, *134* (15), 6776−6784.
(23) Eggleston, C. M.; Ehrhardt, J. J.; Stumm, W. *Am. Mineral.* **1996**, *81*, 1036.
(24) Nesbitt, H. W.; Scaini, M.; Hochst, H.; Bancroft, G. M.; Shaufuss, A. G.; Szargan, R. *Am. Mineral.* **2000**, *85*, 850.
(25) Buckley, A. N.; Woods, R. *Appl. Surf. Sci.* **1987**, *27*, 437.
(26) Nesbitt, H. W.; Muir., I. J. *Geochim. Cosmochim. Acta* **1994**, *58*, 4667.
(27) Amyes, T.; Diver, S.; Richard, J.; Rivas, F.; Toth, K. *J. Am. Chem. Soc.* **2004**, *126*, 4366.
(28) Jacobsen, H.; Correa, A.; Poater, A.; Costabile, C.; Cavallo, L. *Coord. Chem. Rev.* **2009**, *253*, 687.
(29) Tommasi, I.; Sorrentino, F. *Tetrahedron Lett.* **2005**, *46*, 2141.
(30) Tacconi, N. d.; Chanmane, W.; Dennis, B.; MacDonnell, F.; Boston, D.; Rajeshwara, K. *Electrochem. Solid-State Lett.* **2012**, *15*, B5.